

A remote sensing-based approach for water accounting in the East Rapti River Basin, Nepal

Rajendra L Shilpakar^{1*}, Wim GM Bastiaanssen^{2,3} and David J Molden^{4,5}

¹ Riverine Landscape Research Lab, Geography and Planning, University of New England, Armidale, NSW 2351, AUSTRALIA

² Delft University of Technology, Stevinweg 1, 2600GA Delft, The NETHERLANDS

³ eLEAF and Water Watch Foundation, Generaal Foulkesweg 28, 6703 BS Wageningen, The NETHERLANDS

⁴ International Centre for Integrated Mountain Development, Kathmandu, NEPAL

⁵ Formerly, International Water Management Institute, Colombo, SRI LANKA

* For correspondence, e-mail: rshilpak@myune.edu.au

Accurate estimates of evapotranspiration across different land uses are a major challenge in the process of understanding water availability and uses in a river basin. This study demonstrated a remote sensing-based procedure for accurately generating evaporative depletion and runoff in mountainous areas using Landsat ETM+ images combined with standard hydro-meteorological data. The data was used as a key input into the International Water Management Institute (IWMI)'s water accounting procedure to understand how water is now used, and opportunities for improvements in the future. We found a higher annual actual evapotranspiration from the riparian forest than from irrigated agriculture in the East Rapti River basin of Nepal. Another important finding of our study is that simple rainfall surplus can be a good predictor of river flow at an ungagged site of the East Rapti River basin. The water accounting analysis revealed that there is the potential for further development of water resources in the East Rapti River basin as only 59% of the total available water is depleted. A critical analysis of social and ecological flow requirements downstream is necessary before any development of water resources upstream. This study successfully demonstrated that the key inputs required for evaluating and monitoring the overall water resources conditions in a mountainous river basin can be computed from satellite data with a minimal support from ground information.

Key words: water accounting, remote sensing, SEBAL, evapotranspiration, rainfall surplus, evaporative depletion, East Rapti River basin

Water scarcity in many large river basins of Asia will increase significantly due to rapid urbanization, industrialization, increased need for food and agricultural demands, economic development (CA 2007), and climate change (IPCC 2007). This increase in water demands for human uses, combined with the need to retain sufficient water for environmental uses has placed many river basins under stress (Smakhtin et al. 2004). Increased withdrawal of water for agriculture to meet increasing demands for food will alter river flow patterns and affect other uses such as environmental uses in the ways that are not immediately obvious. Hence, efforts to improve water management require better understanding of current water availability and uses in order to overcome problems of scarcity and competition on a longer time scale.

Researchers have pointed out that new methodologies and terms are needed to describe clearly the actual use and physical losses of utilizable water from a hydrologic system (Willardson et al. 1994, Allen et al. 1997). Water accounting is a tool employed to help users in a hydrological domain to understand their resources. The International Water Management Institute (IWMI) developed a water accounting procedure to classify water balance components into water use categories that reflect the consequences of

human intervention in the hydrologic cycle (Molden 1997, Molden and Sakthivadivel 1999, Cai et al. 2002). IWMI's water accounting framework focuses on supply and total depletion of water as opposed to only withdrawals. Thus, the water accounting framework relies on estimates of actual evapotranspiration, as evaporative depletion (consumption) is a main component of total water depletion in a river basin. Actual evapotranspiration reflects the real conditions in the fields, as opposed to the reference evapotranspiration that pertains to a hypothetical land surface (Allen et al. 1998). An updated version of IWMI's water accounting framework (WA+) is under development (Karimi et al. 2012). WA+ is based on 4 sheets that describe the water resources, water depletion, land and water productivity, and water withdrawals. In this framework, land use and land cover classes and their benefits for agriculture, economy and environment are explicitly described (Karimi et al. 2012). WA+, a remote sensing data based water accounting framework, can be applied when ground data are not available or not accessible.

Accurate estimation of actual evapotranspiration (ET_a) is a key challenge for analyzing water availability and water consumption in a river basin (Perry 2007). ET_a is typically estimated based on climatic parameters recorded

in representative weather stations and extrapolated for the larger area or computed as a residual term in water balance equations. Such approaches lead to significant overestimation of ET_a in water shortage conditions because soil moisture and leaf area development are in reality binding constraints (Bastiaanssen et al. 2007). Remote sensing technologies and techniques show promise for improving estimates of ET_a at different spatial scales and in separating ET_a based on land use (e.g. Allen et al. 2011, Bastiaanssen and Bandara 2001, Kustas et al. 2003). For example, Jackson et al. (1977) performed pioneering work on thermal infrared applications for assessing ET fluxes, which was followed by development of several new ET algorithms using remotely sensed thermal measurements (see reviews by Kustas et al. 2003, Courault et al. 2005, Kalma et al. 2008, Allen et al. 2011). Many of these methods were developed and validated in a flat landscape. Applying them to regions with rough topography where ground truth points are lacking (e.g. Himalayan region) has proved difficult.

Nepal is known to have great water resources potential. The renewable surface water available in the country is estimated to be about 225 billion m^3 per annum (UN 2000). Surface water availability is more than 9,000 m^3 per capita per annum, which is many times more than the 'water stress index' of 1,700 m^3 per capita per annum (Falkenmark et al. 1989, Toure et al. 2012). But the magnitude of annual water availability as presented here may be misleading, as there is high spatial and temporal variability in water availability in Nepal due to the contrast between the swollen rivers typical of summer monsoon and the desiccated land during the dry season. Many people in Nepal remain water insecure, because access to water remains difficult throughout the year for household and agricultural use. To guide decisions regarding the use of water, the relationship between its availability from renewable resources and its consumption must be quantitatively described. The relationship is not straightforward due to the heterogeneity and complexity of hydrological processes, combined with a scarcity of data in most of the river basins and catchments in the country.

This study aims to demonstrate how satellite remote sensing images can be effective in providing the key information on the hydrological behavior of a river basin at various spatial scales, ranging from local catchments to the entire river basin. We focus on the quantification of (i) river flow in ungagged watersheds, and (ii) evaporative depletion by agriculture and the environment (natural vegetation) in a Himalayan river basin.

Materials and methods

Basin setting

The East Rapti River basin, comprising an area of rapid urban and agricultural development and also an important nature conservation area (Chitwan National Park), was selected for demonstrating remote sensing and GIS approach for elucidating current water availability and uses at two scales – entire river basin and the relatively small catchments within the basin. The East Rapti River basin extends from 27°21'23"N to 27°47'00"N latitude and 84°08'43" to 85°11'57"E longitude,

covering a total area of 3,084 km^2 . The East Rapti River originates from a catchment in the Mahabharat mountain range about 25 km southwest of Kathmandu, and merges with the Narayani River, an international river that drains towards India, where it is known as the Gandak (Figure 1). The north-eastern part of the basin is mountainous with a maximum elevation more than 2,600 m amsl, while the elevation of downstream areas in the western part of the basin normally does not exceed 300 m amsl. The East Rapti River joins the Narayani River at an elevation of 140 m amsl.

The climate of the basin is humid and subtropical. The average annual rainfall is 2,008 mm, as estimated from the rainfall data recorded at the seven rainfall stations (see Figure 1) within the basin from 1976–2001. More than 80% of the total annual rainfall occurs during the four month monsoon from June to September. July and August are the wettest months, receiving nearly half of the annual rainfall. The average temperature at Rampur station (181m amsl) during the hottest month, June, is about 30°C. The average daily temperature for the same month at Daman (2,380 m amsl) is only about 18°C. January is the coldest month in the basin with an average daily temperature of 15°C at Rampur and about 7°C at Daman.

More than 80% of the economically active populations are involved in agriculture. However, about 46% of agricultural households own less than 0.5 ha of land indicating the subsistence nature of agriculture (Ghimire et al. 2000). Rain-fed agriculture is practiced in mountainous areas of the basin. In the valleys, water from seasonal streams and tributaries is tapped for supplementary irrigation. In the middle reaches of the basin, known as East Chitwan, more than 94 small irrigation systems exist, providing supplementary irrigation to about 9,500 ha of agricultural land. In the most downstream part of the basin (West Chitwan), irrigation water is drawn from the Khageri Khola (a tributary of East Rapti River) and the Narayani River (Smakhtin and Shilpakar 2005).

The East Rapti River basin lies in row 41 of two adjoining Landsat paths, 141 and 142. Path 141 covers about 85% of the upper part of the East Rapti basin. Because of limited budget available for satellite data purchase, we excluded some downstream portion of the basin for the analysis. In our analysis, we treated the confluence of the East Rapti and Khageri, located about 34.5 km upstream from the actual outlet of the entire basin, as the outlet of a hydrological domain that closely represents the entire basin. For the purposes of basin scale water accounting analysis, the hydrological boundary of the outlet covering an area of 2,217 km^2 was treated as the water-balance domain of the East Rapti sub-basin (or simply "sub-basin" hereafter). Catchment scale analysis was carried out for the three catchments the Rajaiya, Manahari and Lothar (see Figure 1).

GIS and remote sensing data

The primary data used in this study include Landsat 7 Enhanced Thematic Mapper Plus (ETM+) images, a digital elevation model (DEM), and routine weather (e.g. rainfall) and river flow data recorded at seven rainfall stations and three river gauges distributed within and around the basin (Figure 1, Table 1). Landsat images record information from

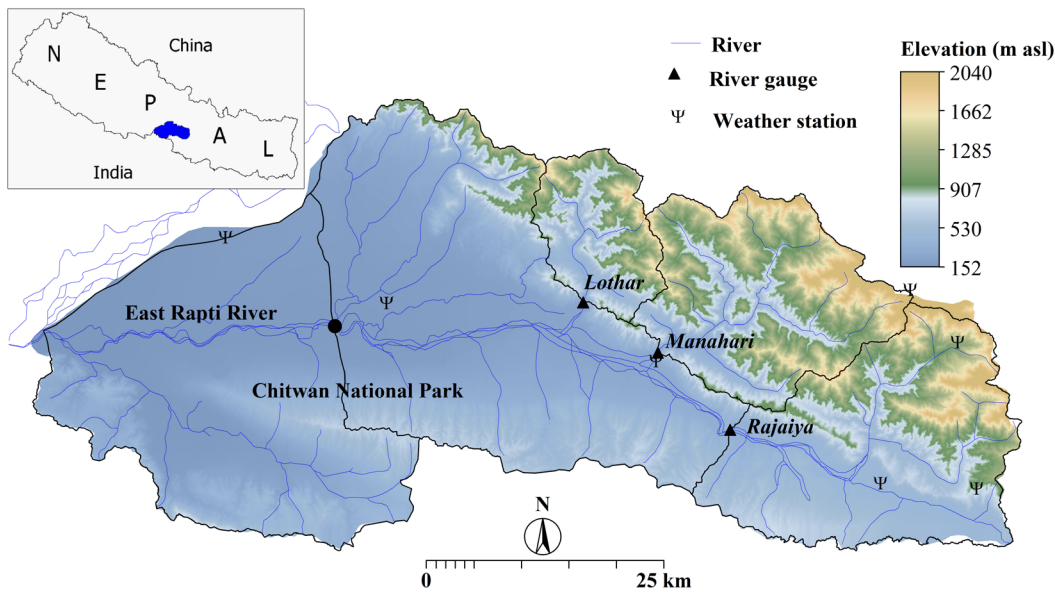


Figure 1. The East Rapti River basin. The inset map shows the position of East Rapti basin within Nepal

Table 1. Overview of the GIS and remote sensing sources and methodologies applied

Technology	Parameter	Original data	Scale/Grid size (m)
GIS	Rainfall	Rain gauge	-
GIS	Terrain elevation	Toposheet	1:25000
GIS	Weather data	Water and Climate Atlas	17,000
RS	Land cover	Landsat ETM+	30
RS	Evapotranspiration	Landsat ETM+ and weather data	30

the visible, near infrared and the thermal infrared region of the electromagnetic spectrum. The information from thermal infrared region is an essential component in estimating energy balance. Three Landsat ETM+ images for path/row 141/41 with <1% cloud cover were acquired for this study. The cloud-contaminated pixels were masked out using a cloud map, which is prepared by analyzing histograms of the visible and thermal bands. The acquisition dates of images, chosen to avoid cloud contamination, were 24 October 2001, 27 December 2001 and 1 March 2002. The long-term rainfall (1976–2001) and river flow data (1963–2001) were acquired from the Department of Hydrology and Meteorology in Nepal. In addition, the hours of sunlight and mean wind speed data were obtained from the Global Water and Climate Atlas (IWMI 2000).

Estimation of actual evapotranspiration (ET_a)

Surface Energy Balance Algorithm for Land (SEBAL) is an algorithm that uses satellite-derived surface albedo, surface temperature and vegetation index, along with routine weather data such as wind speed and humidity, to compute spatial variation in net radiation (R_n), soil heat flux (G_o) and sensible heat flux (H) on a pixel-by-pixel basis (Bastiaanssen et al. 1998, 2002, 2005, Teixeira et al. 2009). The latent heat flux

(λE) is computed as a residual in the surface energy balance equation (Bastiaanssen 2005, Boegh et al. 2002, Senay et al. 2007).

$$\lambda E = R_n - H - G_o \quad [W \cdot m^{-2}] \quad (1)$$

The symbols related to Eq. (1) are explained in the text above. λE is used to estimate the evaporative fraction (Λ).

$$\Lambda = \frac{\lambda E}{R_n - G_o} \quad [-] \quad (2)$$

The ultimate goal of the whole SEBAL process is to compute daily evapotranspiration. The instantaneous evaporative fraction (Λ) is considered similar to its 24-hour counterpart (Shuttleworth et al. 1989, Brutsaert and Sugita 1992). Hence, the SEBAL-derived instantaneous evaporative fraction can be used to compute the actual 24-hour evaporation using Equation 3 (Bastiaanssen et al. 2000).

$$ET_{24} = \Lambda R_{n24} \quad [W \cdot m^{-2}] \quad (3)$$

where ET₂₄ is the 24 hours actual evapotranspiration, R_{n24} is the 24 hours net radiation.

The components of SEBAL are described in detail in Bastiaanssen et al. (1998). A list of equations and symbols involved in SEBAL procedure is provided as **Appendix 1**; an elaborated list of procedures followed in this study is available in Shilpakar (2003). Only the specific terrain related components of the SEBAL will be discussed in this paper (Allen and Tasumi 2000, Tasumi et al. 2000, Morse et al. 2001). The terrain-corrected components include solar radiation for computing net radiation at the land surface (R_n), surface-to-air temperature differences for estimating the sensible heat flux (H), and the psychrometric constant and air density for computing sensible heat flux (H) and latent heat flux (λE).

The solar incident angle is one of the key components of the net radiation at the land surface (R_n). In the mountainous landscape, the value of solar incident angle (θ) is highly dependent on surface slope and aspect. Hence, **Equation 4** needs to be applied for computing cosine of θ for non-flat surface. It computes the solar incident angle for each pixel separately (at $30\text{m} \times 30\text{m}$ pixel resolution to match with Landsat data) and incorporates the effect of slope and aspect for an instantaneous time scale (see Duffie and Beckman 1991, Allen et al. 2007).

$$\cos\theta = \sin\delta \cdot \sin\phi \cdot \sin\sigma - \sin\delta \cdot \cos\phi \cdot \sin\sigma \cdot \cos\gamma + \cos\delta \cdot \cos\phi \cdot \cos\sigma \cdot \cos\omega + \cos\delta \cdot \sin\phi \cdot \sin\sigma \cdot \cos\gamma \cdot \cos\omega + \cos\delta \cdot \sin\phi \cdot \sin\sigma \cdot \sin\omega \quad [-] \quad (4)$$

where δ is the declination of the earth (positive in summer in northern hemisphere), ϕ is the latitude of the pixel in radians (positive for northern hemisphere), σ is the slope in radians, where $\sigma = 0$ is horizontal and $\sigma = \pi/2$ is vertical downward (σ is always positive and represents a downward slope in any direction), γ is the deviation of the normal to the surface from the local meridian, where $\gamma = 0$ for aspect that is due south or the south facing slope, and $\gamma = \pm\pi$ represents a north-facing slope with $\gamma = -$ for east and $\gamma = +$ for western aspect (e.g. $\gamma = -\pi/2$ represents an east facing slope and $\gamma = +\pi/2$ represents a west-facing slope), and ω is the hour angle, where $\omega = 0$ at solar noon, ω is negative in morning, and ω is positive in afternoon.

Using the slope and aspect corrected cosine of solar incident angle, the total instantaneous extra-terrestrial solar radiation K_a^\downarrow for each pixel can be computed using **Equation 5**.

$$K_a^\downarrow = G_{sc} \cdot d_r \cdot \cos\theta \quad [\text{W}\cdot\text{m}^{-2}] \quad (5)$$

where, G_{sc} is the solar constant [$1,367 \text{ Wm}^{-2}$], d_r is the inverse relative earth–sun distance in astronomical units [AU].

By integrating incoming radiation from sunrise to sunset, we can compute the total incoming extra-terrestrial solar radiation K_{a24}^\downarrow for 24 hours using **Equation 6**.

$$K_{a24}^\downarrow = G_{sc} \cdot d_r \cdot \int_{\omega_1}^{\omega_2} \cos\theta \cdot d\omega \quad [\text{W}\cdot\text{m}^{-2}] \quad (6)$$

where ω_1 and ω_2 are start- and end-sun hour angles indicating when the Sun's rays first strike and disappear from the Earth's surface.

For a horizontal surface, ω_1 and ω_2 are equal to $-\omega_s$ and ω_s , where ω_s is the sunset hour angle. Allen and Tasumi (2000) suggest that Equation 6 can be solved for each half-hour time step during the day, and then integrated numerically. Here, the value of ω varies from $-\pi$ to π radian by increments of $0.5\pi/12$ radian.

Estimation of H requires an estimate of the surface-to-air temperature difference (dT_a). In SEBAL, dT_a is estimated as a linear function of surface temperature. Surface temperature was computed from the thermal infrared band of Landsat 7 images (i.e. Band 6). For mountainous landscapes, band 6 in Landsat needs to be adjusted to a common reference elevation for an accurate prediction of dT_a . Otherwise, high elevations that appear to be “cool” will be associated with evaporative cooling. Therefore, a “lapsed” surface-temperature map was made to assist in computing surface-to-air temperature differences. A pixel in the flat area (Chitwan valley) with an elevation of 181 m was identified as a datum for computing the lapsed surface temperature as follows:

$$T_{o_dem} = T_o + 0.0065 \cdot \Delta z \quad [\text{K}] \quad (7)$$

where T_o is the surface temperature in K derived from band 6 of the Landsat image and Δz is difference between the pixel's value (elevation) and the elevation of the datum in meter.

The surface-to-air temperature difference (dT_a) map is a key input for computing the sensible heat flux (H). Assuming, the dT_a has a linear relation to the lapse temperature T_{o_dem} , the surface-to-air temperature difference map can be computed using **Equation 8**.

$$dT_a = a + b \cdot T_{o_dem} \quad [\text{K}] \quad (8)$$

where a and b are internal constants that prescribe the sensible heat flux (H) to remain in a range defined by the user.

The constants a and b can be estimated using the “internal calibration” procedure as explained by Allen et al. (2007). In the process, the lower end of dT_a is associated with “wet pixel having $dT_a=0$ ”, where most available energy is dissipated as latent heat flux (λE). At the higher end, which is associated with “hot pixel with maximum dT_a ”, where the available energy is dissipated to sensible heat flux (H). For the East Rapti River basin, a pixel associated with a well-watered and well vegetated area in the flat valley area near the river was considered as “wet pixel”. A pixel in the dry sandy areas in the river bed was identified as “hot pixel”.

Atmospheric pressure (P) is another parameter required to compute actual evapotranspiration from remote sensing

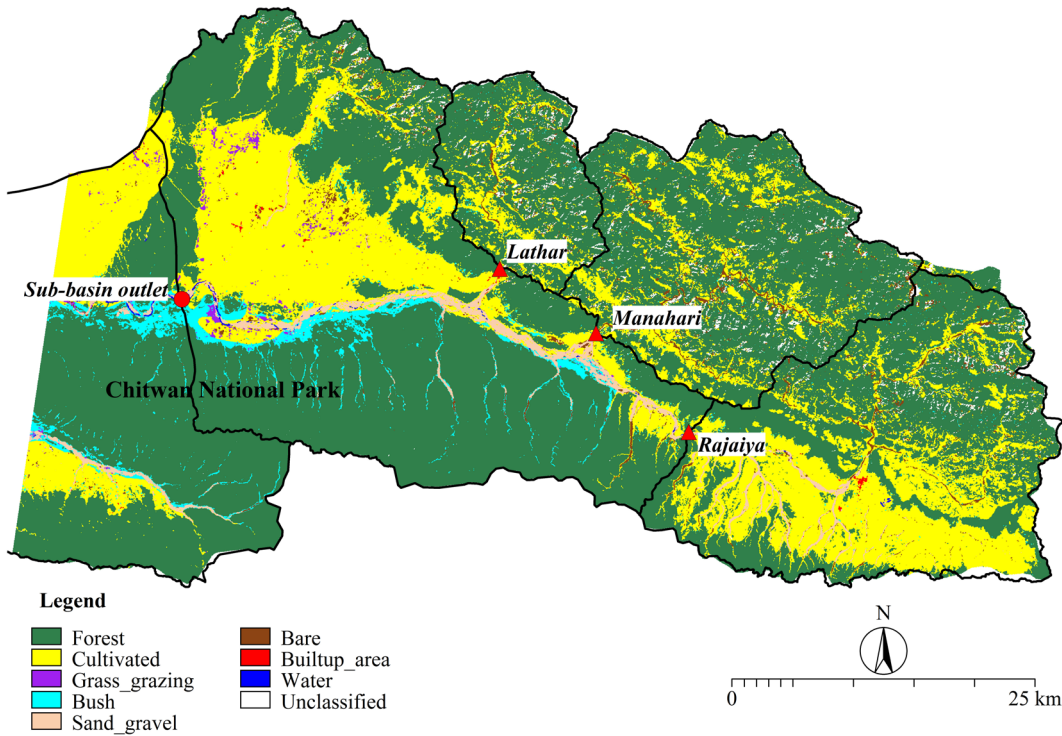


Figure 2. Land cover map of the study area derived from the landscape data used in this study

data. The atmospheric pressure was computed from the elevation data (i.e. Digital Elevation Model) using Equation 9, as suggested by Allen et al. (1998) for the mountainous landscape:

$$P = 101.3 \left(\frac{293 - 0.0065 \cdot z}{293} \right)^{5.26} \text{ [kPa]} \quad (9)$$

where z is the elevation in meters.

The atmospheric pressure allows the computation of air density (ρ_a), and the psychrometric constant (γ') can then be modeled using Equation 10:

$$\rho_a = P / (T_{kv} \cdot R) \quad [\text{kg}\cdot\text{m}^{-3}] \quad (10)$$

where R is the specific gas constant [$0.287 \text{ kJ kg}^{-1}\text{K}^{-1}$] and T_{kv} is the virtual temperature [K] computed from mean air temperature.

$$\gamma' = \frac{c_p \cdot P^{-3}}{\varepsilon \cdot \lambda} \quad [\text{kPa}\cdot\text{C}^{-1}] \quad (11)$$

where c_p is the air specific heat [$\text{J kg}^{-1} \text{C}^{-1}$], ε is ratio of molecular weight of water vapor/dry air ($=0.622$), λ is latent heat of vaporization (2.45 MJ kg^{-1}) and P is atmospheric pressure as in Equation 9.

Monthly values of ET_a were computed based on the Penman-Monteith equation for ET_a . The monthly variability is based on information from weather stations (cloud cover, vapor pressure deficit, slope of the saturated vapor pressure curve), and the surface resistance r_s taken from the SEBAL

computations. This procedure follows the principles outlined in Farah (2001). The surface resistance (r_s) for the image dates was computed by solving the Penman-Monteith equation (Equation 12) in an inverse mode using the SEBAL derived latent heat flux as input.

$$\lambda E = \frac{\Delta(R_n - G_o) + \rho_a c_p \frac{(e_s - e_a)}{r_a}}{\Delta + \gamma' \left(1 + \frac{r_s}{r_a} \right)} \quad [\text{W}\cdot\text{m}^{-2}] \quad (12)$$

where $(e_s - e_a)$ is the vapor pressure deficit of the air [kPa], Δ is the slope of the saturation vapor pressure-temperature relationship [$\text{kPa}\cdot\text{C}^{-1}$], and r_a is aerodynamic resistance [$\text{s}\cdot\text{m}^{-1}$].

The r_s is computed for the date of satellite overpass, and it is assumed that the values are representative for the monthly average values during which that image has been acquired. While this assumption can only be verified by analyzing more Landsat images, it can be used as a first approximation of ET_a . A simple linear interpolation technique was used to compute monthly r_s for other months. The minimum r_s values were restricted to $80 \text{ s}\cdot\text{m}^{-1}$ for the wet months having monthly rainfall greater than 200 mm. The outputs from equations (4) to (11) were also incorporated into the Penman-Monteith equation to get monthly ET_a .

We also prepared monthly reference evapotranspiration (ET_o) maps for 12 months following FAO 56 (Allen et al. 1998) with net radiation corrected for slope and aspect. The ratio of ET_a/ET_o , which we term the "relative coefficient," was used to

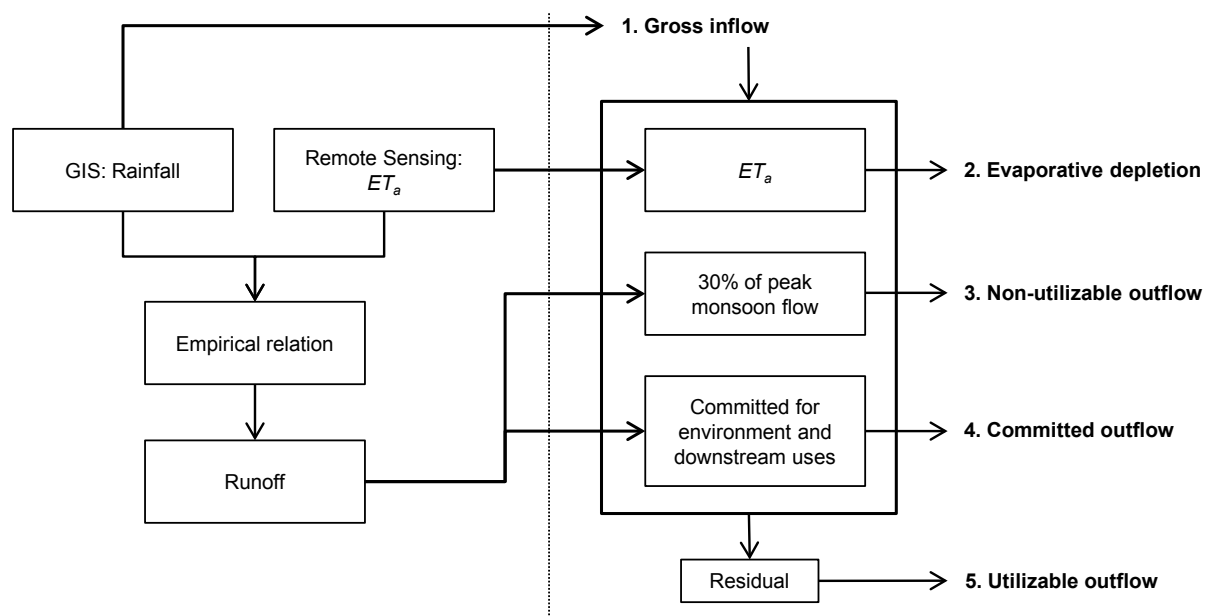


Figure 3. Geo-information procedures for quantifying water accounts, key water accounts derived from Remote Sensing (RS) and Geographic Information System (GIS) process are indicated in right-hand side. ET_a indicates total actual evapotranspiration during the water accounting period.

Table 2. Assumptions and description of key water accounting components considered for current study

Water accounting components	Explanation and assumptions
Gross inflow (GI)	Sum of basin rainfall plus inflow from Bagmati basin (Kulekhani hydro-power)
Net inflow (NI)	For long-term average scenario, NI is assumed to equal to GI, as changes in storage of soil moisture, groundwater, and reservoirs were considered negligible in comparison to other flow components. There are no major reservoirs within the basin.
Process depletion (PD)	Evapotranspiration by crops (ET_a agriculture) plus depletion for domestic, animal and industrial uses
Committed outflow (CO)*	A total of 473 Million m^3 per year for maintaining environmental and tourist activities in the Chitwan National Park (IWMI-Nepal, 2000). 64.1 Mm^3 for diversion to the Khageri irrigation system (IWMI, 1998).
Non-utilizable outflow (NUO)	We attributed 30% of peak monsoon flow (June-September) to NUO within the water balance domain, as it is impossible or difficult to tapped all water discharged during the peak flow period (summer monsoon) by general means of development. Remaining outflow was treated as utilizable outflow (UO).

Available water (AW) NI – CO - NUO

* The contribution of the East Rapti River to the total flow of Narayani (Gandak) River was low compared to those of the other six major tributaries (all originating in the Himalayas). We assumed that water resources development in the East Rapti River will have a nominal downstream effect in India and Bangladesh. Hence, in this study no attempt has been made for computing downstream flow requirement in the East Rapti River for the flow requirements of Narayani River.

indirectly assess performance of SEBAL derived ET_a .

The SEBAL derived monthly ET_a maps were overlaid with a land cover class map (Figure 2) in order to estimate ET_a for each land cover class. The land cover map was derived from the same Landsat images (see Shilpakar 2003). A combination of supervised classification and band ratio method (Meijerink et al. 1994) was applied for the land cover classification using the field sample points collected in October 2002.

Estimation of basin rainfall and river runoff

The distance from the Indian Ocean is an explanatory parameter for the spatial variability of rainfall. An analytical relationship between distance to ocean and rainfall has been established and used as the basis for the determination of spatial distribution of rainfall across the basin. Multiple regression equations for each month were derived using long-term (1976–2001) mean monthly rainfall, elevation,

Box 1. Definition of water accounting components (adapted from Molden, 1997 and Molden and Sakthivadivel, 1999)

Gross inflow (GI) is the total amount of water entering into the water balance domain from precipitation and from surface and subsurface sources.

Net inflow (NI) is the gross inflow plus any changes in storage. If water is removed from the source over the water accounting time period, net inflow exceeds gross inflow; if water is added to storage, net inflow is lower than gross inflow.

Depletion (D) is consumption or removal of water from a water basin that renders it unavailable or unsuitable for further use.

Water is depleted in four ways:

- evapotranspiration, i.e. water is vaporized from surfaces or transpired by plants;
- flow to sink, i.e., water flows into a sea, saline ground water, or other location where it cannot economically be recovered for further use;
- pollution, i.e., water quality is degraded to such an extent that it is not suitable for certain uses;
- incorporation into product, as, for example, the assimilation of irrigation water into plant tissues.

The depletion is **beneficial** if water is depleted in providing an input to produce a good such as an agricultural output, or any other manner deemed beneficial such as ecosystem services. Beneficial depletion can further be classified into *process* and *non-process*. **Process depletion (PD)** is that amount of water which is depleted to produce a human-intended product such as water diverted for crop production, and water consumed by industries. **Non-process depletion (NPD)** occurs when water is depleted naturally (or without human interfered process like irrigation) such as evapotranspiration by natural forests or other natural vegetation. Non-process depletion can be either beneficial or non-beneficial.

Committed outflow (CO) is that part of outflow from the water balance domain that is committed to downstream environmental requirements or downstream water rights.

Uncommitted outflow (UO) is water that is not depleted or committed and is therefore available for use within the domain, but flows out of the basin due to lack of sufficient storage or operational measures. Uncommitted outflow can be classified as utilizable or non-utilizable. Outflow is utilizable if it could be consumed, given improved management of existing facilities. Non-utilizable uncommitted outflow exists when the facilities are not sufficient to capture the otherwise utilizable outflow.

Available water (AW) is net inflow minus both water set aside for committed uses and non-utilizable uncommitted outflow. It represents the quantity of water available for use at the level of basin, service, or use. Available water includes process and non-process depletion plus utilizable outflows.

A **closed basin** is one where all available water is depleted.

An **open basin** is one where there is some uncommitted utilizable outflow.

In a **fully committed basin**, there are no uncommitted outflows. All inflowing water is committed to various uses.

latitude and longitude of the seven rainfall stations within and around the basin (Shilpakar 2003). These monthly regression equations were fitted to estimate the spatial distribution of monthly rainfall for the entire basin using the spatial position (i.e. latitude, longitude) and elevation of each pixel.

Traditionally, river runoff has been estimated from rainfall events, soil properties, antecedent moisture and vegetation cover using empirical equations (Schaake et al. 1996). Bastiaanssen and Chandrapala (2003) suggested a simple and novel method of estimating river runoff using rainfall surplus (rainfall minus evapotranspiration), assuming negligible net infiltration. A similar method was applied in this study in order to estimate river runoff at ungagged sites. The monthly rainfall surplus (Sp) for every pixel was taken as the difference between monthly rainfall (R) and ET_a as follows:

$$Sp = R - ET_a \quad [\text{mm}] \quad (13)$$

The rainfall surplus will not be immediately translated into surface runoff. There is a delayed response in the catchment between rainfall and stream flow due to infiltration, recharge, storage mechanisms, and subsequent interactions between groundwater and surface water. These

delays are accounted for by calculating two-month moving average of monthly rainfall surplus (Sp_{mavg}).

$$Sp_{mavg} = (Sp_{pre} + Sp) / 2 \quad [\text{mm}] \quad (14)$$

where Sp_{pre} is the rainfall surplus for the previous month.

Sp_{mavg} was then used to estimate river runoff depth for the sub-basin by analyzing its relationship with observed runoff depth for the Rajaiya catchment. Out of three gauging stations that measure river flow in the East Rapti River basin (Figure 1), the Rajaiya station was selected for calibrating catchment rainfall surplus, as the river runoff-depth relationship at this catchment can be considered topographically more representative of the sub-basin. The observed river flow data for the Rajaiya station were converted to runoff depth from the catchment on a monthly time scale. The relationship between Sp_{mavg} and runoff depth was used to estimate the runoff depth for the sub-basin (see Shilpakar 2003).

Estimation of water accounting components

The water accounting process described by Molden (1997) and Molden and Sakthivadivel (1999) was followed in this study. The water accounting procedure quantifies total

Table 3. Monthly values of relative coefficients (ET_a/ET_o) for major land cover classes

Land cover	Annual ET_a (mm)	Relative coefficients (ET_a/ET_o)												
		Jan	Feb	Mar	Apr	May	Jun	Jul	Aug	Sep	Oct	Nov	Dec	Annual
Forest	1028	0.83	0.75	0.76	0.76	0.79	0.92	0.98	0.95	1.01	0.92	0.80	0.84	0.86
Cultivated land	960	0.62	0.57	0.60	0.63	0.71	0.90	0.95	0.93	0.97	0.76	0.63	0.63	0.76
Grass/grazing	944	0.56	0.54	0.58	0.61	0.69	0.83	0.90	0.87	0.91	0.60	0.54	0.57	0.71
Bush	1065	0.75	0.69	0.69	0.71	0.77	0.90	0.97	0.94	0.99	0.86	0.75	0.77	0.82
Sand/Gravel	753	0.33	0.34	0.43	0.47	0.58	0.79	0.83	0.80	0.82	0.39	0.33	0.32	0.58
Bare	530	0.34	0.31	0.36	0.38	0.46	0.65	0.68	0.65	0.67	0.36	0.32	0.34	0.49
Built-up area	946	0.55	0.51	0.55	0.59	0.70	0.89	0.95	0.92	0.96	0.61	0.56	0.56	0.72
Water body	1217	0.87	0.81	0.80	0.81	0.86	0.98	1.05	1.02	1.07	0.97	0.85	0.88	0.92
Unclassified	80	0.06	0.04	0.05	0.06	0.09	0.15	0.16	0.13	0.12	0.09	0.06	0.07	0.10

inflows, outflows, and depletions (consumptions) of water within a certain hydrological domain that provide a better picture of water availability and uses in a given hydrological domain (Figure 3). The definitions of major components of water accounting are summarized in Box 1, while the assumptions specific to East Rapti River basin are presented in Table 2.

Three performance indicators were computed in order to refine the analysis of water availability and uses.

- The *depleted fraction of available water* (DFAW) was used to reveal how much scope remains for water resources to be developed and how close they are to being fully committed; it is an indicator of sustainability.
- The *process fraction of available water* (PFAW) was used to indicate how much available water was depleted by processes (agriculture, urban use, and industry).
- The *beneficial utilization of available water* (BUAW) was applied to relate the amount of water depleted by all beneficial uses, both process and non-process, to the amount of water available for use. This indicator offers a more robust view of basin water use than other traditional indicators of efficiency because it takes into consideration the water consumed by valuable natural ecosystems such as National Park, as well as the water consumed by human activities such as agriculture.

The water accounting was calculated for a normal (average) year. The total inflow and outflow components of the water accounting was computed by using the long-term mean monthly rainfall (1976–2001) and mean monthly river flows (1963–2001) data, respectively, while the SEBAL derived ET_a for 2001/02 was considered a normal year evaporative depletion.

Results and discussion

Surface Energy Balance Algorithm for Land

The Surface Energy Balance Algorithm for Land (SEBAL) is used to compute the partitioning of net solar radiation available at the land surface to the sensible heat flux, latent heat flux and the soil heat flux. Energy partitioning can be expressed as the evaporative fraction (Λ). The present study reveals that permanent forest converts a large portion of available energy into latent heat flux for evapotranspiration ($\Lambda > 0.95$). The evaporative fraction for agricultural areas varies from 0.88 (maize) to 0.92 (rice).

Three daily ET_a maps, twelve monthly ET_a maps and one annual ET_a map were prepared using SEBAL. The mean daily ET_a for three Landsat overpass days was found to be 3.2, 1.8 and 3.0 mm d⁻¹ on October 24 and December 27, 2001 and March 1, 2002, respectively. This result is reasonable, as the image dates fell just after the rainy season, when soil moisture was abundant and vegetation was healthy. Due to the low sun elevation on December 27, available energy was low and ET_a was therefore low as well. Another possible reason for the higher ET_a in March as compared to December is the fact that winter crops were only in the developing stage in December while in March they had already well on their way to maturity.

The annual ET_a rates estimated by this study are presented in Figure 4. The ET_a pattern reveals that mountainous catchments exhibit lower ET_a than valley floors in the basin. The highest annual ET_a occurred within the Chitwan National Park in the lower part of the basin. The Lothar and Manahari catchments consist mainly of mountainous areas, whereas the Rajaiya catchment consists of mountainous area as well as a small flat valley. The Rajaiya has slightly higher ET_a than the Lothar and Manahari. The Chitwan valley is comprised of intensive farming areas and protected forests, which had greater annual ET_a than the upper reaches of the basin but slightly lower than that of the Chitwan National Park area.

Table 3 summarizes the monthly ET_a in terms of land cover types. Forest cover showed an average annual average

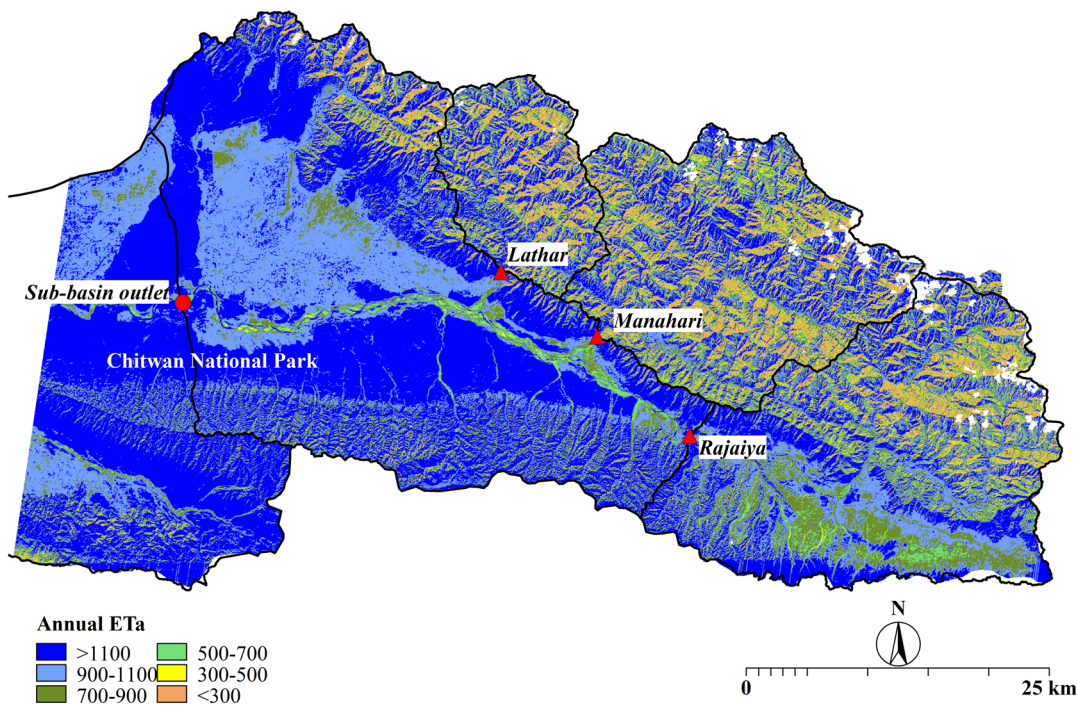


Figure 4. Spatial patterns of annual ET_a in the East Rapti sub-basin (mm y^{-1}) during June 2001 to May 2002.

ET_a of 1,028 mm for the entire sub-basin. It is interesting to note that the highest annual ET_a was found in the foothill forests oriented towards the sunlit slopes (Figure 4). Higher solar radiation per unit area on the sunlit slope than on other slopes and abundant soil moisture in the foot hills mainly due to surface flow probably have caused the higher ET_a from the forest located in river valleys than that from surrounding agricultural areas. A maximum annual ET_a of 1,478 mm was found in forest on the sunlit slopes of valleys, where the reference evapotranspiration ET_o for the forest was 1,411 mm. This gives a relative coefficient (i.e. ET_a/ET_o) of 1.05, which is in good agreement with the crop coefficient reported for many fruit trees in well watered condition and forested wetlands (Allen et al. 1998). Water body had an annual ET_a ($1,217 \text{ mm}\cdot\text{y}^{-1}$) with a relative coefficient close to one. Bushlands with mixed vegetation (short woody plants and tall grass), exhibit an average annual ET_a of 1,065 mm. This slightly higher ET_a than agriculture lands may be because the bushland has an aerodynamically rough surface. However, the extent of bush area in our study area was relatively low and the contribution to the total ET_a of the basin is limited. Agricultural lands showed an average annual ET_a of 960 $\text{mm}\cdot\text{y}^{-1}$ with ET_a/ET_o of 0.76. The lowest ET_a was as low as 1 $\text{mm}\cdot\text{d}^{-1}$ for the areas associated with unclassified land use class, the shadows in steep slope areas where there was no direct sun light. Equation 1 corrects for the effect of slope and aspect in incoming radiation from the sun, but it does account for diffused atmospheric radiation. Consequently, our calculations of ET_a for those pixels may be too low.

According to a previous study (IWMI-Nepal 2000), the average annual ET_a in the East Rapti River basin was 390 mm for agricultural land, 718 mm for dense forest, and 629 mm

for grassland. These figures were significantly lower than the estimates from this study. In previous study, ET_a was computed based on effective rainfall (i.e., the proportion of rainfall that reached the ground) and ET_o . The ET_a was taken to be equal to ET_o if effective rainfall was equal to or greater than ET_o ; otherwise, ET_a was taken to be equal to effective rainfall except in the case of fully irrigated areas, where ET_a must always be equal to ET_o . The main error in previous method is that it does not account for ET from soil moisture during the months with lower levels of effective rainfall. Only 7% of the average annual rainfall occurs during the period from October to June; consequently, evapotranspiration contributions during this period come from the root zone depth soil moisture, a factor not accounted for in previous ET estimates. Another potential error derives from the fact that calculations of ET_o at the reference station (located in Chitwan valley) do not take into account the large spatial variations in climatic condition across the basin.

Using terrain-corrected ET_o and SEBAL-derived ET_a , we computed the relative coefficient (ET_a/ET_o) for each land cover type (Table 3). A monthly relative coefficient close to one indicates that ET_a and ET_o are similar, which is physically possible if the soil is wet and fully covered by vegetation. The identification of wetness and vegetation cover on the basis of ET_a/ET_o was used in assessing SEBAL-derived ET_a for a longer period (Allen et al. 2011). The relative coefficients (ET_a/ET_o) were lowest in dry months, gradually increased from May till September when rainfall occurs, and then decreased again after the monsoon period. The monsoon starts in mid-May and cultivation of summer paddy starts in June. This explains the increase in the relative coefficient during the monsoon period.

A different way to validate the confidence of the ET_a values is by inferring the surface resistance r_s and comparing it to published values of r_s in the international literature (Bastiaanssen and Bandara, 2001). The average values of r_s for paddy and forest in East Rapti sub-basin were estimated to be $77 \text{ s}\cdot\text{m}^{-1}$ and $56 \text{ s}\cdot\text{m}^{-1}$ respectively. There is no monitoring of r_s value in the East Rapti region nor we could find any value previously reported in the literature for this region; consequently, we were unable to validate the estimated r_s values directly. However, our estimates for paddy and forest are consistent with values reported in other regions. For example, Harazono et al. (1998) found daytime rice resistance values ranging between 78 and $111 \text{ s}\cdot\text{m}^{-1}$ in Okayama (Japan). Kelliher et al. (1995) reported a r_s value of $77 \text{ s}\cdot\text{m}^{-1}$ for tropical rain forest. Bastiaanssen and Bandara (2001) found $63 \text{ s}\cdot\text{m}^{-1}$ for mountain forest and $66 \text{ s}\cdot\text{m}^{-1}$ for homesteads in the Kirindi Oya basin of Sri Lanka.

It is interesting to note that the annual ET_a from irrigated lands is actually less than the ET_a from adjacent riverine forests in the river valleys (Figure 4). This indicates that ET_a from riverine forests is at or near its potential, whereas ET_a in the adjacent agriculture area varies based on the growth stage of crops. The agriculture lands remain non-vegetated between crops, which may also have attributed to reduced annual ET_a for the agriculture areas. This may indicate that, at the annual scale, expansion of irrigated agriculture along riverine landscapes does not have a substantial impact on downstream flow in the East Rapti sub-basin. However, at a monthly or finer time scale the prevailing cropping pattern may alter flow pattern.

River runoff

The scatter plot (Figure 5) showed a high statistical correlation ($r^2=0.967$) between average monthly Sp and observed runoff (outflow in mm). The combination of a negative value of the surplus rainfall and positive runoff in Figure 5 indicate that from November to April, river flow was derived primarily from groundwater discharge, i.e. base flow. The estimated runoff along with SEBAL-derived ET_a and GIS-estimated sub-basin rainfall were used in estimating monthly inflow and outflow for the water accounting of the sub-basin. The “residual term” is the difference between all inflows and outflows plus depletions. We found an annual residual term of -23 mm for the East Rapti sub-basin, which came to about 1% of the gross precipitation of 2,011 mm. This indicates that our water balance calculation adequately reflects reality at the sub-basin scale. Comparison of observed and estimated long-term river runoff for the Manahari catchment reveals that estimated runoff is consistent with observed runoff during dry months, while the model underestimates peak flows (Figure 6). The underestimation of peak flow will have less influence on the overall performance indicators because a large portion of peak flow was considered non-utilizable in our water accounting assumptions (see non-utilizable outflow in Table 2). It can be concluded from this analysis that in absence of short and long term water storage options, river runoff can be estimated as a function of rainfall minus ET_a . This may be a breakthrough in approaching the problem of lack of flow records in ungagged basins (Thompson et al.

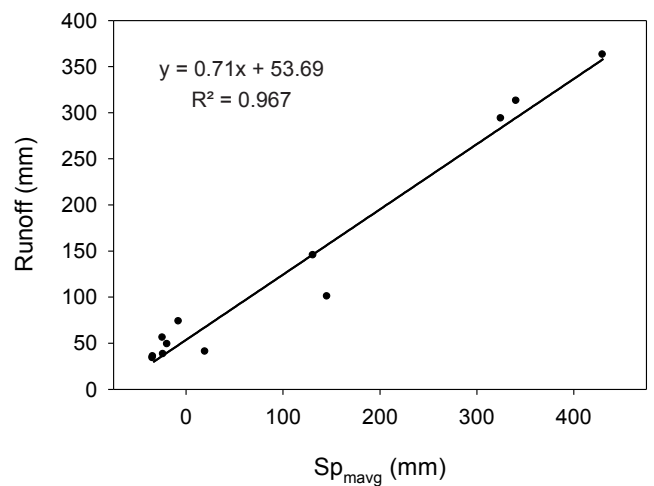


Figure 5. Scatter plot of monthly rainfall surplus and runoff for the Rajaiya watershed; Sp_{mavg} is the average of the surplus rainfall of preceding month and current month (Equation 14)

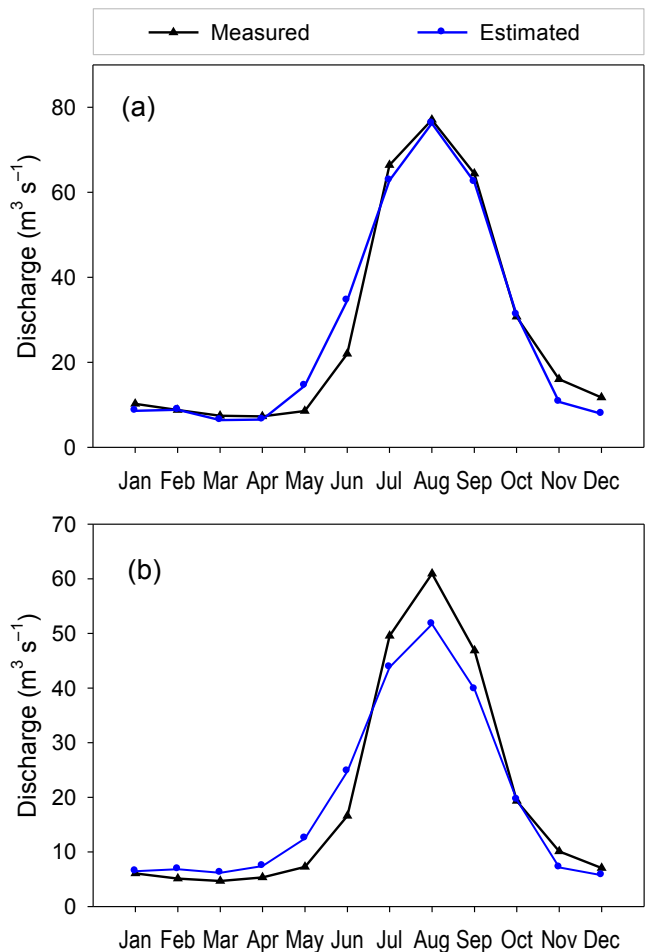
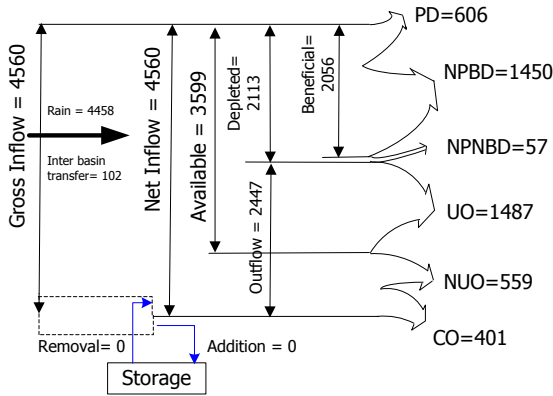
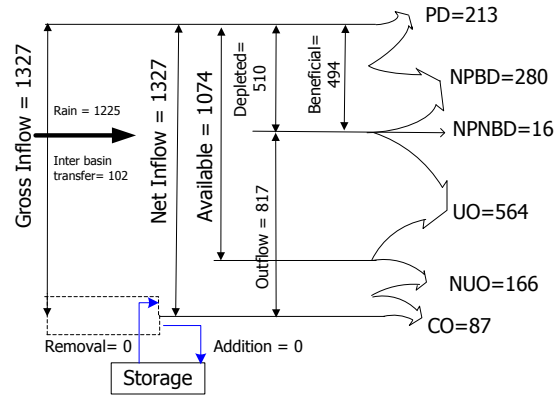


Figure 6. Observed and estimated long-term mean monthly river flow. The estimated monthly flows were computed using a simple linear model of rainfall surplus and runoff (see Figure 5): a) for Rajaiya gauging station, and b) for Manahari gauging station

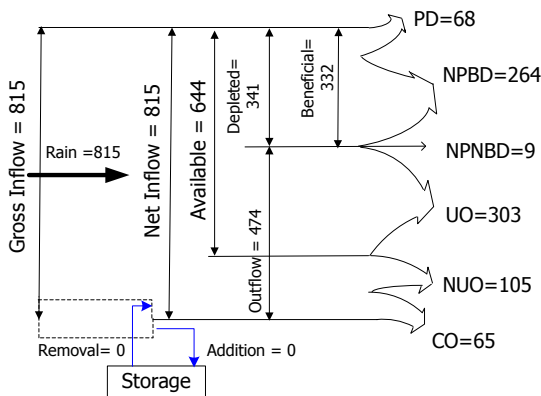
(a) East Rapti sub-basin



(b) Rajaiya catchment



(c) Manahari catchment



(d) Lothar catchment

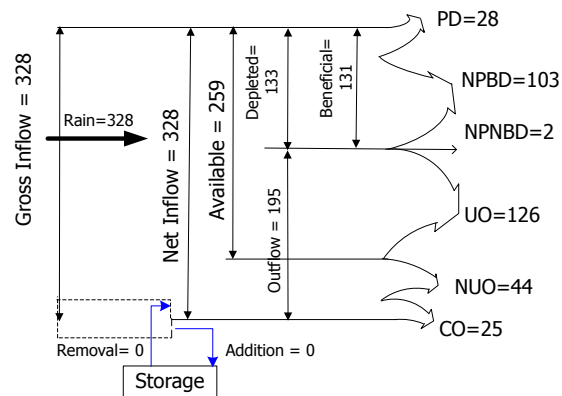


Figure 7. Flow diagrams showing water account results (PD= Process Depletion, NPBD= Non-Process Beneficial Depletion, NPNBD= Non-Process Non-Beneficial Depletion, UO= Utilizable, NUO= Non-Utilizable Outflow, CO= Committed Outflow). The water balance residual term which is about 1% of the gross inflow at sub-basin scale, was adjusted in Net Inflow for computation of water balance components. Hence, there were some minor differences between values for Gross Inflow and Net Inflow although no change in storage. The values are in million cubic meters (Mm³).

2011), a persistent and prevalent constraint in evaluating water resource management conditions at the scale of the river basin.

Water accounting components

We used the hydrological boundary of the confluent Khageri and East Rapti Rivers to define the hydrological domain of our water accounting analysis. Three catchments, Rajaiya, Manahari, and Lothar, were selected for catchment scale water accounting analysis. **Table 2** illustrates water accounting components and a description of assumptions adopted for water accounting of the East Rapti sub-basin.

Water accounting results for the sub-basin and the selected catchments are illustrated in **Figure 7** and the computed indicators are presented in **Table 4**. Our water accounting analysis demonstrates that only 59% of the available water was depleted within the domain of the East Rapti sub-basin, while the remaining 41% of available water leaves the sub-basin as utilizable outflow (**Figure 7a**). Since utilizable outflow from the sub-basin takes place throughout

the year, the East Rapti sub-basin is an ‘open basin’. On the catchment scale, a slightly smaller proportion of the available water was depleted within the domain than in the sub-basin (**Figure 7b, c, and d**). The East Rapti sub-basin may have a potential for further water resource development without adverse downstream effect. However, caution is required as no critical analysis of downstream environmental flow requirements currently exists for the basin despite a preliminary analysis by Smakhtin and Shilpakar (2005) and Smakhtin et al. (2006).

The process fraction of available water was found to be 17% for the sub-basin, which indicates that only a small portion of available water was depleted by human intended processes (**Table 4**). A slightly higher value (20%) was found for Rajaiya, while both Manahari and Lothar showed smaller process fractions of available water (11%). This was due to the fact that the Rajaiya catchment included the municipality of Hetauda as well as the Hetauda Industrial Area. The beneficial utilization of available water was 57% for the sub-basin and 46%, 52% and 51% for the Rajaiya, Manahari and Lothar

Table 4. Water accounting indicators at different spatial scales in the East Rapti sub-basin

Indicator	Definition	East Rapti sub-basin	Rajaiya	Manahari	Lothar
Depleted fraction of available water (DFAW)	Total depletion/ Available Water	0.59	0.47	0.53	0.51
Process fraction of available water (PFAW)	Process depletion/ Available water	0.17	0.20	0.11	0.11
Beneficial utilization of available water (BUAW) or basin efficiency (BE)	Beneficial depletion/ Available water	0.57	0.46	0.52	0.51

catchments, respectively. The similarity of the numbers for beneficial fraction and total depleted fraction indicates a near total absence of non-beneficial depletion in the East Rapti sub-basin.

Summary and conclusions

A rational water management plan cannot be undertaken without understanding where and how much water is available and where and how much water is consumed in a given river basin. Water accounting is a procedure for classifying water balance components into water use categories; it helps planners understand water depletions and unutilized outflows. One paramount factor in water accounting analysis is data availability on actual evapotranspiration. This study shows that SEBAL, supplemented by a mountain radiation model, can be applied in assessing evaporative depletion in the mountain environment where remotely sensed satellite data are available. This study reveals that annual ET_a from the perennial vegetation of the river valleys is higher than that of adjacent agriculture areas. Without remote sensing technology, this phenomenon could only be identified after intensive in situ measurements with advanced instrumentation.

Another important aspect of this water resources research study is the prediction of stream flow. A high statistical correlation ($r^2=0.96$) between Sp_{mveg} and river runoff was found for the East Rapti sub-basin. Thus, rainfall surplus appears to be a simple proxy of river runoff, and this characteristic can be employed to estimate runoff at ungagged sites in East Rapti River basin, provided that storage mechanisms are well understood. Spatially distributed data on rainfall surplus deserves more attention in calculating stream flow estimates in ungagged watersheds, and it is an attractive alternative to (i) empirical solutions of runoff coefficients, (ii) inclusion of sophisticated distributed hydrological models, and (iii) installation of expensive hydro-meteorological stations. The combination of remotely sensed land use and water use information together with rainfall data and a digital elevation model from GIS systems gives us the capability to assess the major terms required for water accounting.

Our water accounting analysis in the East Rapti sub-basin showed that it is an open basin as there was year round outflow of utilizable flow. Only 59% of available water was depleted in the sub-basin. The remaining 41% of available

water is leaving the sub-basin as utilizable outflow. This indicates that there is a potential for further development of water resources in the basin in order to increase beneficial use of the available water. However, any water resources development in the basin must be supported by a comprehensive analysis of the socio-environmental water requirement for the riverine functions (Smakhtin et al., 2006) as the Chitwan National Park, an internationally recognized natural heritage site (listed as UNESCO world heritage), is located at the downstream of the East Rapti River.

Another way to increase water availability might be to exploit artificial recharge and ground water storage options in the sub-basin. Our analysis of rainfall runoff indicates that a large fraction of the river flow consists of base flow (± 40 mm/month). More than 90% of the annual rainfall occurs in a six month period (May–October). In the other six months, rainfall is very low and does not contribute to surface runoff. Because of the close interaction between dry weather flow and ground water storage, it is necessary to investigate and understand the interaction between river flow and ground water storage.

We have demonstrated that the remote sensing images with some routine weather and river flow data can be potentially used to compute water accounting components at different scale of a river basin such as entire basin, sub-basin and smaller catchments. Recent advances in the retrieval of rainfall information from dedicated radar satellites and digital elevation from multi-angular spectral reflectance will further increase our capacity to prepare water accounts for any catchment in the world regardless of ground data coverage.

Acknowledgements

This manuscript is abstracted from the Master's thesis of the first author. The authors are thankful to the Netherlands Fellowship Program for an MSc scholarship to the first author, and to the ITC, the Faculty of Geo-information Science and Earth Observation, University of Twente, the Netherlands and the International Water Management Institute (IWMI) for covering the purchase of Landsat images and other supports during the field works in Nepal in 2002. We would like to acknowledge the anonymous reviewers for their critical comments, which greatly improved this manuscript.

References

Allen R, A Irmak, R Trezza, JMH Hendrickx, W Bastiaanssen and J Kjaersgaard. 2011. Satellite-based ET estimation in agriculture using SEBAL and METRIC. *Hydrological Processes* 25: 4011–4027

- Allen RG, M Tasumi, A Morse, R Trezza, JL Wright, W Bastiaanssen, W Kramber, I. Lorite and CW Robison. 2007. Satellite-based energy balance for mapping evapotranspiration with internalized calibration (METRIC) – applications. *Journal of Irrigation and Drainage Engineering-ASCE* 133: 395–406
- Allen RG and M Tasumi. 2000. Appendix B: Algorithms for applying SEBAL to sloping or mountainous areas. *Application of the SEBAL methodology for estimating consumptive use of water and stream flow depletion in the Bear River basin of Idaho through remote sensing*. Idaho Department of Water Resource. Retrieved on August 2002 from http://www.idwr.state.id.us/gisdata/ET/final_sebal_page.htm
- Allen RG, LS Pereira, D Dirk Raes, and M Smith. 1998. Crop evapotranspiration: guidelines for computing crop water requirements. Rome, Italy. *FAO irrigation and drainage paper* 56. <http://www.fao.org/docrep/X0490E/x0490e00.htm>.
- Allen RG, LS Willardson and HD Fredriksen. 1997. *Water use definitions and their use for assessing the impacts of water conservation*. In JM deJager, LP Vermes and R Ragab (eds.): The Proceedings of The International Commission on Irrigation and Drainage (ICID) Workshop: 'Sustainable Irrigation in Areas of Water Scarcity and Drought,' pp 72–80. Oxford, England, 11–12 September 1997
- Bastiaanssen WGM, EJM Noordman, H Pelgrum, G Davids, BP Thoreson and RG Allen. 2005. SEBAL model with remotely sensed data to improve water-resources management under actual field conditions. *Journal of Irrigation and Drainage Engineering* 131 (1): 85–93
- Bastiaanssen, W and L Chandrapala. 2003. Water balance variability across Sri Lanka for assessing agricultural and environmental water use. *Agricultural Water Management* 58 (2): 171–192
- Bastiaanssen WGM, A Mobin-ud-Din, and Y Chemin. 2002. Satellite surveillance of evaporative depletion across the Indus Basin, *Water Resources Research* 38: 1273–1282
- Bastiaanssen WGM and KMPS Bandara. 2001. Evaporative depletion assessments for irrigated watersheds in Sri Lanka. *Irrigation Science* 21: 1–15
- Bastiaanssen WGM. 2000. SEBAL-based sensible and latent heat fluxes in the irrigated Gediz Basin, Turkey. *Special Issue, hydrological models and field data. Journal of Hydrology* 229 (1–2): 87–100
- Bastiaanssen WGM, M Menenti, RA Feddes and AAM Holtslag. 1998. A remote sensing surface energy balance algorithm for land (SEBAL): 1. Formulation. *Journal of Hydrology* 213 (1–4): 198–212
- Bastiaanssen WGM, RG Allen, P Droogers, G D'urso and P Steduto. 2007. Twenty-five years modeling irrigated and drained soils: State of the Art. *Agricultural Water Management* 92(3): 111–125
- Boegh E, H Soegaard, and A Thomsen. 2002. Evaluating evapotranspiration rates and surface conditions using Landsat TM to estimate atmospheric resistance and surface resistance. *Remote Sensing of Environment* 79: 329–343
- Brutsaert W and M Sugita. 1992. Application of self-preservation in diurnal evolution of the surface budget to determine daily evaporation. *Journal of Geophysical Research* 97: 377–382
- CA [Comprehensive Assessment]. 2007. Water for food, water for life: a comprehensive assessment of water management in agriculture, Molden, David. (Ed.), London, UK: EARTHSCAN; Colombo, Sri Lanka: International Water Management Institute. 645p
- Cai X, DC McKinney and L Lasdon. 2002. A framework for sustainability analysis in water resources management and application to the Syr Darya Basin, *Water Resources Research* 38 (6): 1085–1099
- Courault D, B Seguin and A Olioso. 2005. Review about estimation of evapotranspiration from remote sensing data: from empirical to numerical modeling approach. *Irrigation and Drainage Systems* 19: 223–249
- Duffie JA and WA Beckman. 1991. *Solar engineering of thermal process*. New York: John Wiley and Sons. 919 p
- Falkenmark M, J Lundqvist, and C Wildstrand. 1989. Macro-scale water scarcity requires micro-scale approaches: aspects of vulnerability in semi-arid development. *Natural Resources Forum* 13 (4): 258–267
- Farah HO. 2001. *Estimation of regional evaporation under different weather conditions from satellite and meteorological data: A case study in the Naivasha basin, Kenya*. PhD dissertation. ITC dissertation 80. Wageningen University, Wageningen. 170p
- Ghimire DP, JP Dutta, R Poudel, TB Khatri-Chetri, KR Adhikari, A Sukla, G Upreti, and B Devkota. 2000. *Socio-economic and stakeholders analysis in the East Rapti River basin of Nepal*. Water Management Study Program, Institute of Agriculture and Animal Sciences, Rampur, Nepal and International Water Management Institute, Sri Lanka. *Unpublished report*. 39p
- Harazono Y, J Kim, A Miyata, T Choi, Ji Yun and JW Kim. 1998. Measurement of energy budget components during the International Rice Experiment (IREX) in Japan. *Hydrological Processes* 12: 2081–2092
- IPCC [International Panel on Climate Change]. 2007. Fourth Assessment Report – Climate Change 2007: Synthesis Report. Summary for Policymakers
- IWMI [International Water Management Institute]. 1998. *Comparative performance assessment in 7 selected schemes in Nepal*. International Water Management Institute, Colombo, Sri Lanka; Research and Technology Development Branch (RTDB), DOI, Kathmandu, Nepal and Ford Foundation, Delhi, India. *Unpublished report*.
- IWMI [International Water Management Institute]. 2000. *World Water and Climate Atlas*. International Water Management Institute. <http://www.cgiar.org/iwmi/WAtlas/atlas.htm>. Accessed in January 2003
- IWMI-Nepal [International Water Management Institute, Nepal]. 2000. *Water accounting for East Rapti River basin of Nepal*. Kathmandu, Nepal: Research and Technology Development Branch (RTDB)/DOI, Institute of Agriculture and Animal Science (IAAS), and International Water Management Institute (IWMI). *Unpublished report*.
- Jackson RD, RJ Reginato and SB Idso. 1977. Wheat canopy temperature: a practical tool for evaluating water requirements. *Water Resources Research* 13: 651–656
- Kalma J, T McVicar and M McCabe. 2008. Estimating land surface evaporation: A review of methods using remotely sensed surface temperature data. *Surveys in Geophysics* 29: 421–469
- Karimi, P, D. Molden, W. Bastiaanssen, and X. Cai. 2012. Water accounting to assess use and productivity of water: evolution of a concept and new frontiers In J. Godfrey and K. Chalmers (Eds.). *Water Accounting: International Approaches to Policy and Decision-making*. pp 76–90. Edward Elgar Publishing Limited, Cheltenham UK
- Kelliher FM, R Leuning, MR Raupach and ED Schultze. 1995. Maximum conductances for evaporation from global vegetation types. *Agriculture and Forest Meteorology* 73: 1–16
- Kustas WP, GR Diak and MS Moran. 2003. Remote sensing of evapotranspiration, in M. Dekkers (ed.), *Encyclopedia of Water Science*: 267–274
- Meijerink AMJ, JAM de Brouwer, CM Mannaerts and CR Valenzuela. 1994. *Introduction to the use of geographic information systems for practical hydrology*. Enschede, The Netherlands: ITC. 243p
- Molden D and R Sakthivadivel. 1999. Water accounting to assess use and productivity of water. *International Journal of Water Resources Development* 15 (1–2): 55–71
- Molden D. 1997. *Accounting for Water Use and Productivity*. SWIM Paper 1: International Water Management Institute (IWMI), Colombo, Sri Lanka. 16p
- Morse A, RG Allen, M Tasumi, WJ Kramber, R Trezza and JL Wright. 2001. *Final Report: Application of the SEBAL Methodology for Estimating Evapotranspiration and Consumptive Use of Water through Remote Sensing*. Idaho Department of Water Resources. University of Idaho, Department of Biological and Agricultural Engineering. http://www.idwr.state.id.us/gisdata/ET/final_sebal_page.htm. Accessed in August 2002.
- Perry CJ. 2007. Efficient irrigation; inefficient communication; flawed recommendations. *Irrigation and Drainage* 56: 367–378
- Schaake JC, VI Koran, QY Duan, K Mitchell and F Chen. 1996. Simple water balance model for estimating runoff at different spatial and temporal scales. *Journal of Geophysical Research* 101: 7461–7475

Senay, GB, M Budde, JP Verdin and M Melesse. 2007. A coupled remote sensing and simplified surface energy balance approach to estimate actual evapotranspiration from irrigated fields. *Sensors* 7: 979–1000

Shilpakar RL. 2003. *Geo-information Procedures for Water Accounting: A Case of the East Rapti River Basin, Nepal* [MSc thesis]: International Institute for Geo-information Science and Earth Observation (ITC), the Netherlands. 59 p. (http://www.itc.nl/library/Papers_2003/msc/wrem/shilpakar.pdf)

Shuttleworth WJ, RJ Gurney, AY Hsu and JP Ormsby. 1989. FIFE: the variation in energy partitioning at surface flux sites, remote sensing and large scale global processes. *Proceedings of the Baltimore Symposium IAHS publication no. 186*, IAHS Press, Oxfordshire, p 67–74

Smakhtin VU and RL Shilpakar. 2005. Planning for environmental water allocations: An example of hydrology-based assessment in the East Rapti River, Nepal. *Research Report 89*. Colombo, Sri Lanka: International Water Management Institute (IWMI). 20p

Smakhtin VU, RL Shilpakar and DA Hughes. 2006. Hydrology-based assessment of environmental flows: an example from Nepal. *Hydrological Sciences* 51 (2): 207–222

Smakhtin VU, C Revenga and P Doll. 2004. Taking into account environmental water requirements in global-scale water resources assessments. *Comprehensive Assessment of Water Management in Agriculture Research Report 2*, Colombo, Sri Lanka: International Water Management Institute (IWMI), Comprehensive Assessment Secretariat. 24 p.

Tasumi M, RG Allen and W Bastiaanssen. 2000. Appendix A:

The theoretical basis of SEBAL. *Application of the SEBAL methodology for estimating consumptive use of water and stream flow depletion in the Bear River basin of Idaho through remote sensing*. Idaho Department of Water Resource. http://www.idwr.state.id.us/gisdata/ET/final_sebal_page.htm. Accessed in August 2002.

Teixeira AH de C, WGM Bastiaanssen, MD Ahmad and MF Bos. 2009. Reviewing SEBAL input parameters for assessing evapotranspiration and water productivity for the low-middle São Francisco River basin, Brazil: Part a: Calibration and validation. *Agricultural and Forest Meteorology* 149: 462–476

Thompson S, C Harman, P Reed, A Montanari, A Schumer, G Bloschl, L Marshall, E Istanbuluoglu, P Trock, J Shaman, D Niyogi, L Band, H Savenije, A Shatre and J Wilson. 2011. *Predictions under change (PUC): Water, Earth and Biota in the Anthropocene*. <http://cwaces.geog.uiuc.edu/synthesis/reports/documents/AppendixE-PUCDraftReport.pdf>

Toure NM, A Kane, JF Noel, V Turmine, V Nedeff and G Lazar. 2012. Water–poverty relationships in the coastal town of Mbour (Senegal): Relevance of GIS for decision support. *International Journal of Applied Earth Observation and Geoinformation* 14:33–39

UN [United Nations]. 2000. *Assessment of water resources and water demand by user sector in Nepal*. New York, United Nations. 126p

Willardson LS, RG Allen and HD Frederiksen. 1994. Universal fractions for the elimination of irrigation efficiency, paper presented at the 13th Technical Conference of USCID, Denver, Colorado, October 19–22, 1994

Appendix 1. A list of equations and symbols involved in SEBAL procedures

$$1. \quad r_p = \frac{\pi \cdot L_\lambda \cdot d_r^2}{E_{sun_\lambda} \cdot \cos \theta} \quad [-]$$

$$2. \quad r_{toa} = \sum c_{p_i} \cdot r_{p_i} \quad [-]$$

$$3. \quad r_o = \frac{r_{toa} - r_{path_radiance}}{\tau_{sw}^2} \quad [-]$$

$$4. \quad \tau_{sw} = 0.75 + 2x10^{-5} \cdot z \quad [-]$$

$$5. \quad NDVI = \frac{r_4 - r_3}{r_4 + r_3} \quad [-]$$

$$6. \quad SAVI = \frac{(1 + L_1)(r_4 - r_3)}{L_1 + r_4 + r_3} \quad [-]$$

$$7. \quad \varepsilon_o = 1.009 + 0.047 \cdot \ln(NDVI) \quad [-]$$

$$8. \quad T_b = \frac{K_2}{\ln\left(\frac{K_1}{L_\lambda} + 1\right)} \quad [K]$$

$$9. \quad T_o = \frac{T_b}{\varepsilon_o^{0.25}} \quad [K]$$

$$10. \quad T_{o_dem} = T_o + 0.0065 \cdot \Delta z \quad [K]$$

$$11. \quad R_n = \lambda E + H + G_o \quad [W \cdot m^{-2}]$$

$$12. \quad Rn = (1 - r_o)K^\downarrow + (L^\downarrow - L^\uparrow) - (1 - \varepsilon_o) \cdot L^\downarrow \quad [W \cdot m^{-2}]$$

$$13. \quad K^\downarrow = G_{sc} \cdot \cos \theta \cdot d_r^{-2} \cdot \tau_{sw} \quad [W \cdot m^{-2}]$$

$$14. \quad L^\downarrow = 1.08 \cdot (-\ln \tau_{sw})^{0.265} \cdot \sigma \cdot T_{o_ref}^4 \quad [W \cdot m^{-2}]$$

$$15. \quad G_o = R_n \cdot \left\{ \frac{(T_o - 273)}{r_o} \cdot [0.0032 \cdot (c_1 \cdot r_o) + 0.0062 \cdot (c_1 \cdot r_o)^2] \cdot (1 - 0.978 \cdot NDVI^4) \right\} \quad [W \cdot m^{-2}]$$

$$16. \quad H = \frac{\rho_a \cdot C_p}{r_{ah}} \cdot dT_a \quad [W \cdot m^{-2}]$$

$$17. \quad \frac{1}{u_*} = \frac{\ln\left(\frac{z_b}{z_{om}}\right)}{k \cdot u_b} \quad [s \cdot m^{-1}]$$

Z_b is under all conditions 100 m, so you can replace Z_b by 100.

$$18. \quad z_{om} = \exp(-5.809 + 5.62SAVI) \quad [m]$$

$$19. \quad r_{ah} = \frac{1}{k \cdot u_*} \ln\left\{ \frac{z_{ref}}{z_{oh}} \right\} \quad [s \cdot m^{-1}]$$

Z_{ref} is under all conditions 2 m, so you can replace Z_{ref} by 2.0; Z_{oh} is under all conditions 0.1 m, so you can replace z_{oh} by 0.1.

$$20. \quad dT_a = a + b \cdot T_{o_dem} \quad [K]$$

$$21. \quad L = -\frac{\rho_a C_p \cdot u_*^3 T_{o_dem}}{k \cdot g \cdot H} \quad [m]$$

22.

$$\psi_m = 2 \ln\left(\frac{1+x_m}{2}\right) + \ln\left(\frac{1+x_m^2}{2}\right) - 2ARCTAN(x_m) + 0.5\pi$$

[-]

23. $\psi_h = 2 \ln\left(\frac{1+x_h^2}{2}\right)$ [-]

24. $x_m = \left(1 - 16 \frac{z_{blend}}{L}\right)^{0.25}$ [-]

z_{blend} is always 100.

25. $x_h = \left(1 - 16 \frac{z_{ref}}{L}\right)^{0.25}$ [-]

z_{ref} is always 2.

26. $\frac{1}{u_*} = \frac{\ln\left(\frac{100}{z_{om}}\right) - \psi_m}{k \cdot u_{100}}$ [$s \cdot m^{-1}$]

27. $r_{ah} = \frac{\ln\left\{\frac{z_{ref}}{z_{oh}}\right\} - \psi_h}{k \cdot u_*}$ [$s \cdot m^{-1}$]

z_{ref} is always 2 m.

28. $\Lambda = \frac{R_n - G_o - H}{R_n - G_o}$ [-]

39. $ET_{24} = \Lambda R_{n24}$ [$W \cdot m^{-2}$]

30. $R_{n24} = (1 - r_o) \cdot \tau_{sw24} \cdot K_{a24}^{\downarrow} - 110 \tau_{sw24}$ [$W \cdot m^{-2}$]

Symbol	Representation	Unit
L_λ	Spectral radiance	$W \cdot m^{-2} \cdot sr^{-1} \cdot \mu m^{-1}$
r_p	Spectral reflectance	-
r_3 and r_4	Spectral reflectance at band 3 (0.63–0.69 μm) and band 4 (0.76–0.90 μm)	-
d_r	Earth-Sun distance	AU
$E_{sun,\lambda}$	Solar spectral irradiance	$W \cdot m^{-2} \cdot \mu m^{-1}$
θ	Solar incident angle	Rad
r_{toa}	Albedo at top of the atmosphere	-
r_o	Broad band surface albedo	-
$r_{path_radiance}$	Albedo path radiance	-
τ_{sw}	One way transmittance	-
z	Elevation	m
$NDVI$	Normalize difference vegetation index	-
$SAVI$	Soil adjusted vegetation index	-
L_1	The non-dimensional correction factor	-
ϵ_o	Surface emissivity	-
T_b	Brightness temperature	K
K_1, K_2	Constants (for ETM+: $K_2 = 1282.71$ and $K_1 = 669.09$)	-
T_o	Surface temperature	K
T_{o_dem}	Lapsed surface temperature (DEM corrected apparent surface temperature)	K
Δz	Difference of a pixel's elevation from the datum	m
R_n	Net radiation	$W \cdot m^{-2}$
λE	Latent heat flux	$W \cdot m^{-2}$

H	Sensible heat flux	$W \cdot m^{-2}$
G_o	Soil heat flux	$W \cdot m^{-2}$
K^\downarrow	Incoming shortwave radiation	$W \cdot m^{-2}$
L^\downarrow	Incoming longwave radiation	$W \cdot m^{-2}$
L^\uparrow	Outgoing longwave radiation	$W \cdot m^{-2}$
G_{sc}	Solar constant [$1367 W m^{-2}$]	$W \cdot m^{-2}$
σ	Stefan Boltzman constant	
T_{o_ref}	Surface temperature at a reference point	K
c_1	A factor to convert the instantaneous values of albedo to daily averages ($c_1 = 1.1$)	-
ρ_a	Air density	
C_p	Specific heat of air at constant pressure ($1004 J kg^{-1} K^{-1}$)	$J \cdot kg^{-1} \cdot K^{-1}$
r_{ah}	Aerodynamic resistance to heat transport	$s \cdot m^{-1}$
dT_a	Vertical difference in air temperature between layers $z = z_{oh}$ and $z = z_{ref}$	K
z_{oh}	Surface roughness length to heat transport	M
z_{ref}	Reference height	M
u_*	Local scale friction velocity	$m \cdot s^{-1}$
u_b	Average wind speed at blending height b	$m \cdot s^{-1}$
k	von Karman's constant (0.41)	-
z_{om}	Surface roughness for momentum transport	M
a and b	Constants	-
L	Monin-Obukhov stability length	M
g	Acceleration due to gravity	$m \cdot s^{-2}$
ψ_m	Stability correction factor for buoyancy effects on the momentum flux	-
ψ_h	Stability correction factor for heat flux	-
Λ	Evaporative fraction	-
ET_{24}	Daily (24 hours) actual evapotranspiration	$W \cdot m^{-2}$ [or $mm \cdot d^{-1}$]
R_{n24}	Daily net radiation	$W \cdot m^{-2} \cdot d^{-1}$
K_{a24}^\downarrow	Daily incoming extraterrestrial solar radiation	$W \cdot m^{-2} \cdot d^{-1}$
τ_{sw24}	Daily atmospheric transmittance	-